

# **Cigarette butt-derived carbons have ultra-high surface area and unprecedented hydrogen storage capacity**

*Troy Scott Blankenship and Robert Mokaya\**

University of Nottingham, University Park, Nottingham NG7 2RD, U. K.

E-mail: r.mokaya@nottingham.ac.uk

## Abstract

Discarded cigarette filters, in the form of cigarette butts, are a major waste disposal and environmental pollution hazard due to mainly containing cellulose acetate which is non-biodegradable; 5.8 trillion cigarettes are smoked worldwide per annum generating > 800 000 metric tons of cigarette butts. Apart from causing litter, cigarette butts contain contaminants such as toxic heavy metals, which can leach into waterways, potentially causing harm to both humans and wildlife. In an effort to turn dangerous waste into value products, this study explores the valorisation of discarded smoked cigarette filters/butts. We show that porous carbons derived from cigarette butts, via sequential benign hydrothermal carbonisation and activation, are super porous and have ultra-high surface area ( $4300 \text{ m}^2 \text{ g}^{-1}$ ) and pore volume ( $2.09 \text{ cm}^3 \text{ g}^{-1}$ ) arising almost entirely (> 90%) from micropores. The carbons also have uncharacteristically high oxygen content associated with O-containing functional groups (COOH, C-OH and C=O), and show anomalous behaviour with respect to the effect of activation temperature on porosity, the latter being ascribable to the chemical mix present in cigarette butts and their hydrochar products. Due to the combined effects of high surface area, high microporosity and an oxygen-rich nature, the carbons exhibit unprecedentedly high hydrogen storage capacity of 8.1 wt% excess uptake, and 9.4 wt% total uptake at  $-196 \text{ }^\circ\text{C}$  and 20 bar, rising to total uptake of 10.4 wt% and 11.2 wt% at 30 and 40 bar, respectively. The hydrogen storage capacity is the highest reported to date for any porous carbons and attains new levels for porous materials in general. This work also raises the question on whether valorisation can solve the intractable cigarette butt problem.

## 1. Introduction

Hydrogen is an attractive energy source especially for motor vehicles due to its high gravimetric energy capacity as well as the fact that it does not produce any CO<sub>2</sub> emissions.<sup>1-7</sup> Hydrogen may be used to produce energy via a hydrogen fuel cell, which is a redox cell wherein the chemical energy of hydrogen is converted to electrical energy through use of an oxidising agent (usually oxygen).<sup>7,8</sup> An alternative to using a hydrogen fuel cell in a car is to burn the hydrogen in a manner similar to that of a combustion engine.<sup>9,10</sup> Targets, for the year 2020, set by the United States Department of Energy (DOE) for hydrogen-powered cars include gravimetric energy of 1.8 kWh kg<sup>-1</sup> (5.5 wt% H<sub>2</sub>), and energy density of 1.3 kWh L<sup>-1</sup> (0.040 kg L<sup>-1</sup>).<sup>11</sup> Solid state materials are considered to be a viable route to achieving the required level of hydrogen storage.<sup>12-14</sup> Storage materials currently under investigation can be divided into two main groups, the first of which store hydrogen via chemisorption, including, for example, metal hydrides,<sup>15</sup> while the second group use physisorption and are typically highly porous materials with a high surface area such as carbons,<sup>16-30</sup> metal organic frameworks (MOFs)<sup>31-37</sup> and covalent organic frameworks (COFs).<sup>38-40</sup> It is now well established that the hydrogen storage capacity of porous solid state materials is dependent on surface area (with high area favouring good uptake) and the presence of micropores.<sup>16-59</sup> In terms of porosity, optimised hydrogen storage materials should possess high surface area that arises from micropores.

The ongoing search for new materials is a key factor in attempts to achieve the hydrogen storage targets required to make the mooted Hydrogen Economy a reality.<sup>12-40</sup> The search for new hydrogen stores targets materials that have new or improved properties, are easier or cheaper to prepare, and that are sustainable. Improved properties can be engendered by tailored design based on knowledge of what is required for hydrogen storage, while sustainability may be achieved via valorisation routes with respect to the starting materials.

As part of our on-going search for carbon materials with optimised properties for hydrogen storage, we have recently shown that cellulose-based precursors are good starting materials for such porous carbons.<sup>20,22</sup> This is of particular interest, with respect to valorisation of waste materials, because a cellulose derivate (i.e., cellulose acetate) is the principal component of cigarette filters.<sup>60,61</sup> The import of this connection is that discarded cigarette filters, in the form of cigarette butts, are currently a major waste disposal and environmental pollution hazard because cellulose acetate, though photodegradable (in the presence of TiO<sub>2</sub>) is not biodegradable.<sup>62-67</sup> The number of cigarettes smoked worldwide per annum tops 5.8 trillion and generates in the order of 800 000 metric tons of cigarette butts.<sup>63,68</sup> For example, disposed cigarette filters (butts) make up the majority, by mass, of litter found on beaches.<sup>69</sup> A further hazard are the contaminants, especially toxic heavy metals, present in cigarette filters, which leach into waterways, potentially causing harm to both humans and wildlife.<sup>70-72</sup> It is therefore clear that cigarette butts need to be taken out of the environment. It would be highly desirable if the cigarette butts, rather than being disposed of, are converted to a high value product via a valorisation process. Given that they are mainly composed of cellulose acetate, the aforementioned factors make cigarette butts waste a particularly attractive starting material for valorisation to porous (e.g., activated carbons). This would be in line with the current trend to move away from coal-based carbonaceous precursors to biomass-derived or waste-based starting materials for activated carbon synthesis.<sup>16</sup>

There has previously been some interest in the use of cigarette filters as starting material for the formation of porous carbons. Polarz *et al* carbonised cellulose acetate from cigarette filters to generate lowly porous (surface area of 262 m<sup>2</sup> g<sup>-1</sup> and pore volume of 0.21 cm<sup>3</sup> g<sup>-1</sup>) non-graphitic carbons.<sup>73</sup> Chen *et al* prepared *p6mm* mesostructured carbonaceous materials with surface area of 526 m<sup>2</sup> g<sup>-1</sup>, pore volume of 0.59 g cm<sup>3</sup> g<sup>-1</sup> and pore width of 5.1 nm via an evaporation-induced self-assembly method using cigarette filters as matrix

scaffold.<sup>74</sup> Lee *et al* prepared micro-mesoporous carbon with surface area of 573 m<sup>2</sup> g<sup>-1</sup> from carbonisation of cigarette filters, while samples carbonised under ammonia had higher surface area of 1634 m<sup>2</sup> g<sup>-1</sup>.<sup>75</sup> However, as far as we are aware, there has so far been no report on preparation of activated carbons from cigarette filters or waste cigarette butts. In this study we explore the preparation of activated carbons from cigarette filters and discarded cigarette butts and assess the hydrogen uptake capability of the resulting carbons. This study unravels some unexpected and anomalous trends between activating conditions and the properties, especially porosity, of the resulting activated carbons and how this affects hydrogen uptake capacity. We discuss the findings in terms of how the chemical mix present in cigarette butts affects the activation process.

## **2. Experimental Section**

### **2.1 Materials synthesis**

Used cigarette filters/butts were collected to form the precursor for the S (smoked) group of carbons. Unused (or 'fresh') filters that were used to generate the F group of carbons were obtained from purchased cigarettes (of similar brand as S group) following separation of the filter from the cigarette. In both cases, the wrapping paper was removed from the filter, care being taken to avoid contamination with tobacco or ash. The cigarette filters were then ground in a spice grinder to produce a fluffy white or yellow-brown mass, for F and S filters, respectively. The ground cigarette filters were then hydrothermally carbonised by heating a mixture of the filters and water (at a ratio of 1 g filter to 10 mL water) in a stainless steel autoclave to 250 °C at a ramp rate of 5 °C min<sup>-1</sup>, holding at 250 °C for 2 h and then cooling to room temperature at a ramp rate of 5 °C min<sup>-1</sup>. The resulting carbonaceous matter (hydrochar) was recovered and dried at 112 °C. The hydrochars were denoted as FF-hydrochar (fresh filters) or SF-hydrochar (smoked filters).

For the activation a KOH/hydrochar ratio of 4 was used. A ground and homogenous KOH/hydrochar mixture, in alumina boats, was placed in a horizontal furnace and heated under nitrogen to 600, 700 or 800 °C at a ramp rate of 3 °C min<sup>-1</sup>. Samples were held at the target temperature for 1 h and then allowed to cool under nitrogen. The generated activated carbons were recovered by filtration and washed in 2M HCl with stirring at room temperature and then with deionised water until washings had neutral pH. The samples were dried in an oven at 112 °C. The activated carbons were designated as FF-4T (group F, fresh filters) or SF-4T (group S, smoked filters) where 4 is the KOH/hydrochar ratio and T is the activation temperature (600, 700 or 800 °C).

## 2.2 Materials Characterisation

Thermogravimetric analysis (TGA) was performed using a TA Instruments SDT Q600 analyser under flowing air conditions (100 mL/min). Powder XRD analysis was performed using a PANalytical X'Pert PRO diffractometer with Cu-K $\alpha$  light source (40 kV, 40 mA) with step size of 0.02° and 50 s time step. CHN elemental analysis was performed using an Exeter Analytical CE-440 Elemental Analyser. Inorganic (metal) content was determined via ICP-OES analysis using a Perkin Elmer Optima 2000 DV ICP-OES analyser. Temperature programmed desorption (TPD) was performed using a Hiden CATLAB system with He as carrier gas. Infra-red spectroscopy (FTIR) spectra was obtained using a Bruker Alpha FTIR spectrometer. Porosity analysis and determination of textural properties was performed via nitrogen sorption using a Micromeritics 3FLEX sorptometer. Prior to analysis (at -196 °C), the carbons were degassed under vacuum at 200 °C for 12 h. The apparent surface area (hereinafter referred to simply as surface area) was calculated using the Brunauer-Emmett-Teller (BET) method applied to adsorption data in the relative pressure ( $P/P_o$ ) range 0.04 – 0.22. The total pore volume was determined from the nitrogen uptake at close to saturation pressure ( $P/P_o \approx 0.99$ ). The micropore surface area and micropore volume were determined

via *t*-plot analysis. Non-local density functional theory (NL-DFT) was applied to nitrogen adsorption isotherms to determine pore size distribution.

### **2.3 Hydrogen uptake measurements**

Hydrogen uptake capacity of the carbons was measured by gravimetric analysis with a Hiden XEMIS Intelligent Gravimetric Analyser using 99.9999% purity hydrogen additionally purified by a molecular sieve filter. Prior to analysis, the carbon samples were dried for 24 h at 80 °C and then placed in the analysis chamber and degassed at 200 °C and  $10^{-10}$  bar for 4 – 6 h. The hydrogen uptake measurements were performed at -196 °C (in a liquid nitrogen bath) over the pressure range of 0 to 40 bar.

## **3. Results and Discussion**

### **3.1 Elemental Composition and Nature of Carbon**

The starting materials in this study, fresh (FF) or smoked (SF) cigarette filters were first converted to hydrochar (FF-hydrochar and SF-hydrochar, respectively) via hydrothermal carbonisation. Given the nature of cigarette filters (or butts for smoked cigarettes) with respect to their chemical composition, wherein the main component is cellulose acetate along with a host of other additives including metals, we analysed the cigarette butt derived hydrochars and compared them to cellulose acetate-derived hydrochar.<sup>22</sup> Firstly, we determined the carbon content of the FF and SF hydrochars as shown in Table 1 and Table S1. The C and H content of the fresh FF-hydrochar, at 63.6 and 4.2 wt%, respectively, is slightly lower than that of the smoked SF-hydrochar (68.5 and 5.7 wt%, respectively), meaning that the former has a higher oxygen content (32.2 wt%) compared to 24.8 wt% for the latter. It is also noteworthy that the SF-hydrochar contains some N while the FF-hydrochar appears to be N-free. The presence of N in the SF-hydrochar may be explained by nicotine that is trapped in the filters during smoking, while for the fresh un-smoked

cigarettes such trapping is absent. Comparison with CA-hydrochar derived from cellulose acetate (Table S1) shows, in general, a similar C, H, O content to that of the cigarette filter or butt derived hydrochars, which is consistent with the fact that cellulose acetate is the main component of cigarette filters. As shown in Table 1, activation of both the FF and SF hydrochars results in an increase in the C content, with the increase being generally greater at higher activation temperature. On the other hand, the H content decreases significantly, while the oxygen content shows a less drastic reduction. This means that the cigarette filter or butt derived activated carbons possess higher oxygen content (16 – 31 wt%) than is normally observed for activated carbons, including those derived from cellulose (4.4 - 11.5 wt%) but similar to those derived from cellulose acetate.<sup>16,20,22</sup> The SF series of activated carbons also retain some N content of between 0.4 and 1 wt%.

**Table 1.** Elemental analysis of hydrochar derived from fresh (FF-hydrochar) and smoked (SF-hydrochar) cigarette filters, and activated carbons derived from the hydrochars.

Sample	C [%]	H [%]	N [%]	O [%]	(O/C) <sup>a</sup>	(H/C) <sup>a</sup>
FF-hydrochar	63.6	4.2	0	32.2	0.380	0.793
SF-hydrochar	68.5	5.7	1.0	24.8	0.272	1.000
FF-4600	66.9	1.9	0	31.2	0.350	0.340
FF-4700	78.3	0.5	0	21.2	0.203	0.077
FF-4800	82.5	0.4	0	17.1	0.156	0.058
SF-4600	70.5	0.6	1.1	27.8	0.296	0.102
SF-4700	77.6	0.7	0.4	21.3	0.206	0.108
SF-4800	82.8	0.3	0.5	16.4	0.149	0.044

<sup>a</sup>Atomic ratio

The presence and amount of O in the activated carbons was probed using temperature programmed desorption (TPD). The TPD was performed after thermal

evacuation of the carbons at 150 °C, and thus probed the nature of O-functional groups that are stable under such conditions. The TPD profiles for the evolution of CO<sub>2</sub> and CO for the two sets of activated samples are shown in Figure 1. Desorption of CO<sub>2</sub> occurs in the temperature range 150 – 600 °C, and it is noticeable that the temperature of maximum desorption slightly shifts to higher values as activation temperature rises. Desorption of CO is observed within the temperature range of 300 and 900 °C with desorption maxima in the range 600 – 750 °C. The TPD profiles are consistent with the expectation that the CO<sub>2</sub> arises from O-containing functional groups that are thermally less stable, including carboxylic acids, lactones and anhydrides, while the CO is from thermally more stable moieties such as carbonyls, quinonic or phenolic groups.<sup>22,76-78</sup> In general the TPD profiles are similar to those that have previously been reported for activated carbons.<sup>22,76-78</sup> The high oxygen content of the present carbons (16 – 31 wt%) may be evidenced by a comparison of their CO<sub>2</sub> and CO TPD profiles to those of an activated carbon derived from cellulose (designated as C-4700) that has oxygen content of 7.1 wt%.<sup>20</sup> Such a comparison (Figure S1) shows that much higher CO<sub>2</sub> and CO is evolved from the SF-4T carbons compared to sample C-4700, which is consistent with the greater oxygen content of the former. The O-functional groups on the activated carbons were also probed with FTIR. The IR spectra (Figure S2) of the SF-hydrochar and representative activated carbon (sample SF-4600) show several bands arising from O-functional groups, including the following; C–OH stretch band at ca. 3430 cm<sup>-1</sup>, C–OH bend band at ca. 1625 cm<sup>-1</sup>, C–O vibration at 1380 cm<sup>-1</sup>, and C=O peak at 1710 cm<sup>-1</sup>.<sup>22,79-82</sup> The spectra of sample SF-4600 does not, however, exhibit C–H peaks at ca. 2850 and 1450 cm<sup>-1</sup> that are observed for the SF-hydrochar, which is in agreement with the much lower H content of the activated carbon (Table 1). The IR spectra offers further evidence for a high content of oxygen functional groups, which is consistent with the O content of the present carbons.

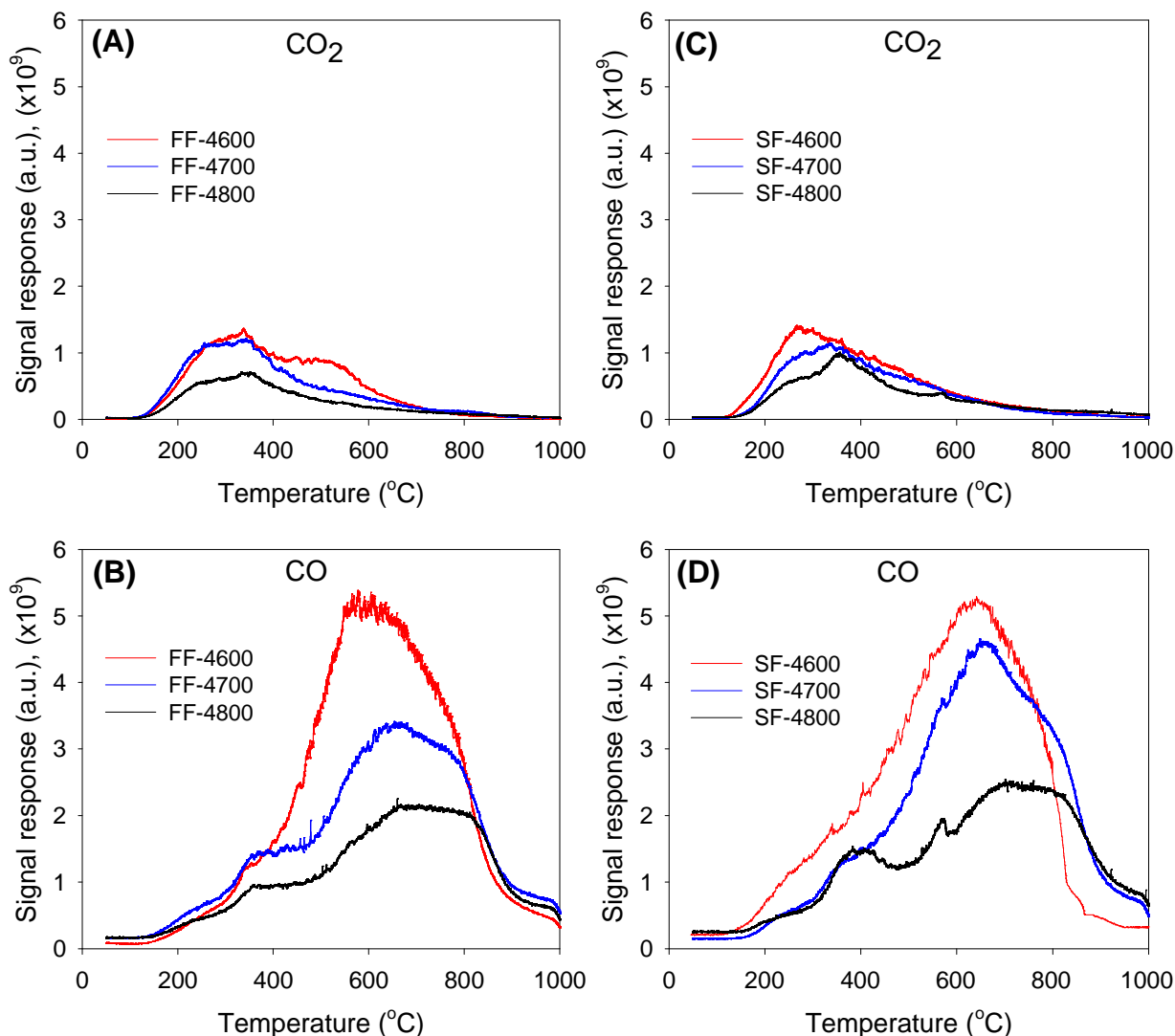


**Figure 1.** Evolution of CO<sub>2</sub> (A, C) and CO (B, D) under TPD conditions for activated carbons derived from fresh cigarette filters (A, B) and smoked cigarette butts (C, D).

Given that cigarettes are known to contain a mix of non-carbonaceous additives, including metals, we performed thermogravimetric analysis of the FF and SF hydrochars in an attempt to gauge the amount of inorganic residue they contain. Figure 2 shows the TGA curves for the FF and SF hydrochars, and CA-hydrochar obtained from pure cellulose acetate. All three hydrochars are stable below 200 °C, after which carbon combustion occurs in a single mass-loss event that is completed at ca. 550 °C. It is interesting to note that the CA-hydrochar was completely burnt off and no residue was left at 600 °C, while the FF-

hydrochar and SF hydrochar had residual mass of ca. 1 and 2 – 2.5 wt%, respectively. We attribute the residual mass to inorganic matter (likely in the form of metal oxides) arising from metal additives that are known to be present in smoked cigarettes filters/butts.<sup>70-72</sup> The smoked SF-hydrochar has higher residual mass as more of the additives are transferred to and trapped in the filters (or butts) when the cigarette is smoked.<sup>70-72</sup> We performed powder XRD analysis of the hydrochars in an effort to establish the presence of crystalline inorganic matter as would be indicated by sharp peaks that are uncharacteristic of porous carbon frameworks. The XRD patterns in Figure 3 show no sharp peaks for the CA-hydrochar, while some peaks are observed in the patterns of the FF and SF hydrochar, with the peaks being more prominent for the SF-hydrochar. Thus the XRD patterns are consistent with the presence of non-carbonaceous matter in the FF and SF hydrochars with the later having greater amounts, which is in agreement with the TGA data in Figure 2. Elemental analysis to determine the metal content of the SF-hydrochar, via ICP-OES, detected (i.e., close to or above 10 ppm) the presence of several metals, including Al, Ba, Cu, Fe, Ca, Na, K, Mg, Mn, and Zn. The most prevalent metals (i.e., close to or greater than 0.1 wt%) were Ca, K, Mg, Na, and Al. This findings are consistent with previous reports on the additives present in cigarette butts.<sup>70-72</sup> Inter alia, the presence of metals (especially K, Na and Ca) in the hydrochars can be expected to influence their activation. This premise is based on the fact that the activating process, for example with KOH, arises from the action of K as activating agent. Indeed, the interesting mix of metal additives present in cigarette filters or butts was part of the motivation for using them as starting materials for activated carbons. We however note that the activated carbons were themselves free of metals or crystalline inorganic residues as indicated by the absence of sharp peaks in their XRD patterns (Figure S3). The extensive post activation washing process appears to remove all inorganic matter.

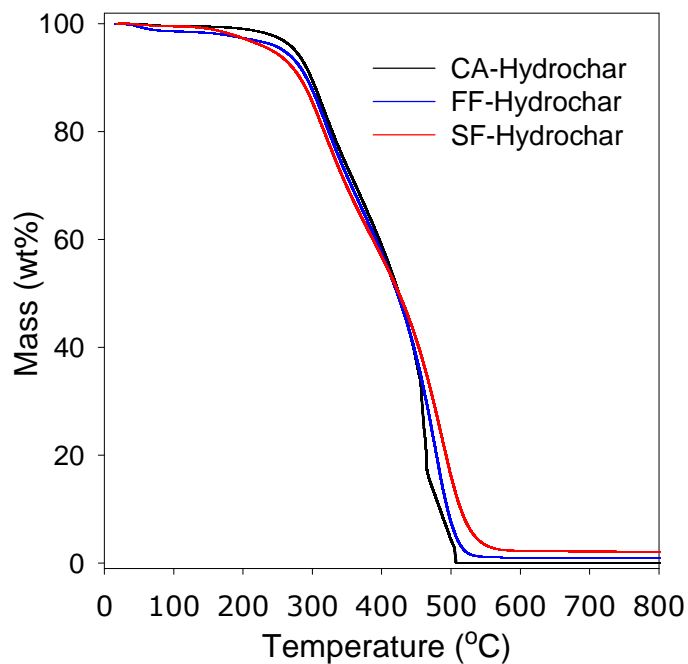


**Figure 2.** Thermogravimetric analysis (TGA) curve of hydrochar derived from fresh (FF-hydrochar) and smoked (SF-hydrochar) cigarette filters, and from cellulose acetate (CA-hydrochar), thermally treated in air.

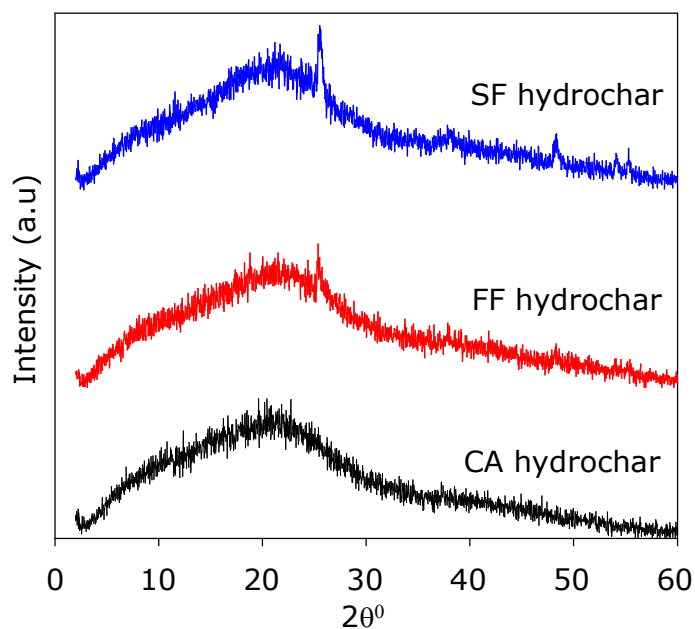


**Figure 3.** Powder XRD patterns of hydrochar derived from fresh (FF-hydrochar) and smoked (SF-hydrochar) cigarette filters, and from cellulose acetate (CA-hydrochar).

### 3.2 Porosity

The porosity of the FF and SF series of activated carbons was probed by nitrogen sorption analysis. The nitrogen sorption isotherms of the FF series of activated carbons are given in Figure 4A. All three FF-4T samples exhibit type I isotherms that are characteristic of microporous materials.<sup>83</sup> The extent of porosity generated, as measured by the amount of nitrogen adsorbed, increases as activation temperature rises from 600 to 800 °C, which is the normal trend usually observed.<sup>16,20,26,84-94</sup> The shape of the isotherms indicates that the pore size increases as activation temperature rises, which is the expected trend in line with the fact that increase in overall porosity in activated carbons is usually accompanied with isotherm changes arising from increase in the amount of nitrogen adsorbed, widening of the adsorption knee and increase in pore size.<sup>16,20,26,84-94</sup> Figure 4B shows the pore size distribution (PSD) curves of the FF-4T carbons, and as expected the pore size distribution broadens as activation temperature rises. The pore size maxima obtained from the PSD curves is summarised in Table 2. Although the small micropores of size  $\leq 1.2$  nm are retained for all the FF-4T carbons, there is a gradual broadening of PSD to larger micropores of size up to 2 nm as activation temperature rises.

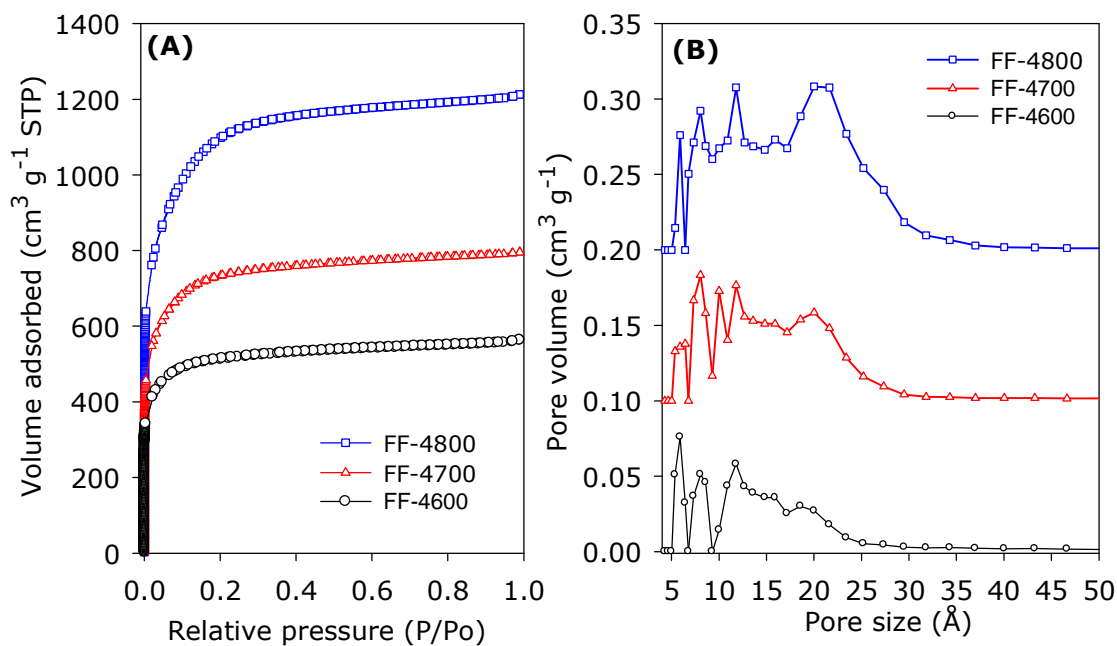


**Figure 4.** (A) Nitrogen sorption isotherms and (B) pore size distribution curves of FF series of activated carbons derived from fresh cigarette filters. See experimental section for sample designation.

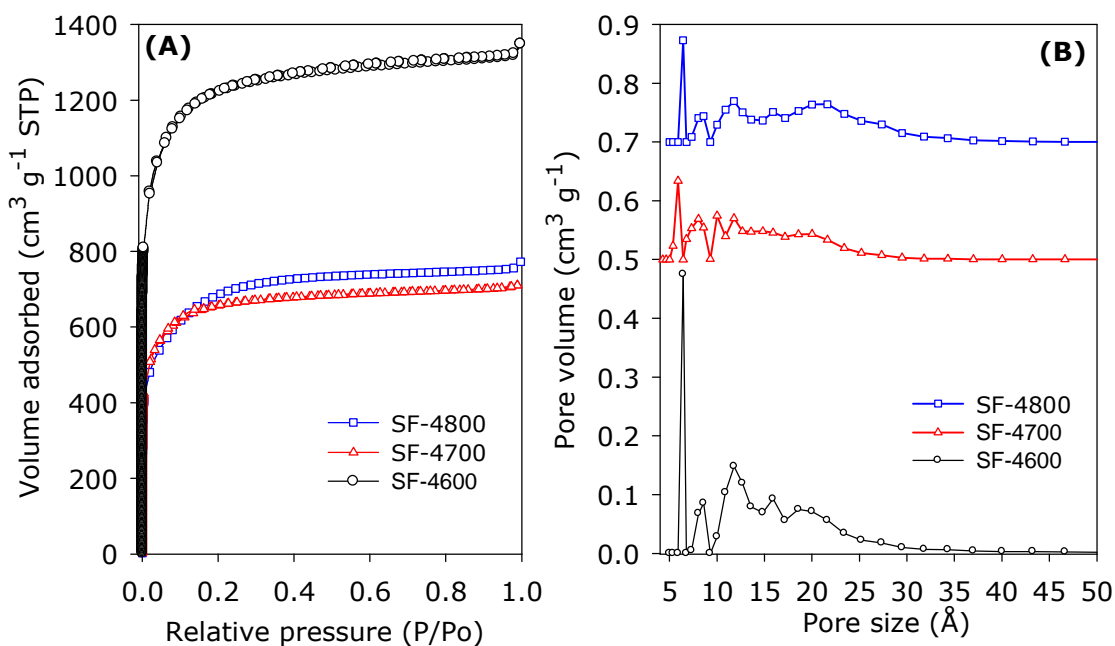


**Figure 5.** (A) Nitrogen sorption isotherms and (B) pore size distribution curves of SF series of activated carbons derived from smoked cigarette filters/butts. See experimental section for sample designation.

The nitrogen sorption isotherms of the SF-4T series of samples prepared from cigarette butts are shown in Figure 5A. All the isotherms are type I and typical for microporous materials. However, the isotherms show an unusual, even anomalous, trend with respect to the effect of activation temperature. The extent of porosity generated, as measured by the amount of nitrogen adsorbed, decreases as activation temperature rises from 600 to 800 °C, which is the reverse of what is observed for FF-4T samples as described above (Figure 4), and is the opposite of what is known to occur for activated carbons.<sup>16,20,26,84-94</sup> For the SF-4T carbons, sample SF-4600 has the highest amount of adsorbed nitrogen. However, the shape of the isotherms suggests that the pore size increases as activation temperature rises. Thus for SF-4T samples, the increase in overall porosity is not in tandem with widening of the adsorption knee and increase in pore size.<sup>16,20,26,84-94</sup> The PSD curves shown in Figure 5B indicate that the pore size distribution broadens as activation temperature rises, but according to the isotherms, this change is accompanied by a *decrease* rather than increase in overall porosity. The increase in pore size of SF-4T carbons at higher activation temperature is clear from the pore size maxima obtained from the PSD curves as summarised in Table 2. Small micropores of size  $\leq 1.2$  nm are retained for all the SF-4T carbons in a manner similar to the FF-4T carbons, along with a gradual increase in the proportion of larger micropores of size up to 2 nm as activation temperature rises. The observed anomalous behaviour (i.e., highest porosity at 600 °C, which then decreases for samples activated at higher temperature), may be explained by the presence of significant amounts of metal additives in the SF-hydrochar as evidenced above by TGA, XRD and elemental analysis data. It is likely that the metal additives (namely, K, Ca, Na, Mg, etc) retained in the hydrochar act as ‘extra’ activating agents in addition to the KOH thus resulting in what may be considered as ‘overactivation’ of the carbons prepared at temperatures higher than 600

°C. The main factors that determine the extent of activation of any carbon precursor under our activation regime are KOH/carbon ratio (i.e., amount of activating agent) and activation temperature. Increase in the KOH/carbon ratio and/or temperature causes greater activation. The two factors need to be judiciously combined to optimise the porosity generated. If the amount of activating agent, temperature or a combination of both is too high, then the activation conditions can be too severe and beyond the optimum conditions, which, in a sense, leads to ‘overactivation’ and a decrease in the porosity generated. Thus, there is a point beyond which the carbon becomes over activated leading to a decrease rather than increase in overall porosity (as indicated by apparent surface area and pore volume) – although the pore size can still rise. We postulate that for SF-4T carbons, activation temperature of 700 and 800 °C leads to over activation due to the ‘added’ activating effect of the metal additives already present in the SF-hydrochar. On the other hand, at 600 °C, the mix of activating agents (KOH and metal additives) is just right to generate what may be described as optimal porosity. The lower amount of metal additives in the FF-hydrochar means that the anomalous behaviour is not observed. The effect of metal additives was evidenced by the fact that simple heating of the non-porous SF-hydrochar at 600 – 800 °C for 1 h in the absence of KOH generated porous carbon (Figure S4) with apparent surface area and pore volume, at 800 °C, of up to 983 m<sup>2</sup> g<sup>-1</sup> and 0.49 cm<sup>3</sup> g<sup>-1</sup>, respectively. Similar heating of the CA-hydrochar (which contains no metal additives) resulted in hardly any increase in porosity.

**Table 2.** Textural properties and H<sub>2</sub> uptake of cigarette butt-derived activated carbons.

Sample	Surface area <sup>a</sup> (m <sup>2</sup> g <sup>-1</sup> )	Pore volume <sup>b</sup> (cm <sup>3</sup> g <sup>-1</sup> )	Pore size <sup>c</sup> (Å)	H <sub>2</sub> uptake <sup>d,e</sup> (wt%)			
				1 bar	20 bar	30 bar	40 bar
FF-4600	1970 (1512)	0.86 (0.59)	6/8/12/18	2.0	5.2 (4.6)	5.6 (4.8)	5.9 (4.9)
FF-4700	2803 (1901)	1.23 (0.73)	6/8/12/20	3.2	7.2 (6.4)	7.8 (6.6)	8.3 (6.7)
FF-4800	4113 (2075)	1.87 (0.79)	6/8/12/21	3.0	8.2 (7.0)	9.1 (7.2)	9.7 (7.3)
SF-4600	4310 (3867)	2.09 (1.71)	6.4/8/12/19	4.0	9.4 (8.1)	10.4 (8.3)	11.2 (8.4)
SF-4700	2512 (2019)	1.20 (0.91)	6/8/12.5/20	2.7	6.8 (6.0)	7.4 (6.2)	7.8 (6.3)
SF-4800	2393 (1810)	1.09 (0.70)	6.4/8/12/21	3.0	6.6 (5.9)	7.2 (6.1)	7.6 (6.2)

The values in the parenthesis refer to: <sup>a</sup>micropore surface area and <sup>b</sup>micropore volume. <sup>c</sup>Pore size distribution maxima obtained from NLDFT analysis. <sup>d</sup>Gravimetric (wt%) H<sub>2</sub> uptake at -196 °C and various pressures (i.e., 1, 20, 30 and 40 bar). <sup>e</sup>The values in parenthesis are excess H<sub>2</sub> uptake.

The textural properties of both FF-4T and SF-4T series of carbons are given in Table 2. For The FF-4T carbons, the apparent surface area rises from 1970 m<sup>2</sup> g<sup>-1</sup> for sample FF-4600 to 2803 m<sup>2</sup> g<sup>-1</sup> for FF-4700 and to a high of 4113 m<sup>2</sup> g<sup>-1</sup> for FF-4800. We note that sample FF-4800 has one of the highest surface areas ever reported for activated carbons.<sup>16,88-96</sup> The pore volume follows a similar trend, rising from 0.86 cm<sup>3</sup> g<sup>-1</sup> for sample FF-4600 to 1.23 cm<sup>3</sup> g<sup>-1</sup> for FF-4700 and 1.87 cm<sup>3</sup> g<sup>-1</sup> for CA-4800. Regarding the proportion of microporosity, the usual trend (decrease in microporosity at high activation temperature) is observed; the proportion of micropore surface area is 77% for FF-4600, and decreases to 68% for FF-4700 and 51% for FF-4800. For micropore volume, the proportions are 69%, 60%, and 42% for FF-4600, FF-4700 and FF-4800, respectively.

For the SF-4T carbons, the apparent surface area is highest at 4310 m<sup>2</sup> g<sup>-1</sup> for sample SF-4600, and then decreases to 2512 m<sup>2</sup> g<sup>-1</sup> for SF-4700 and 2393 m<sup>2</sup> g<sup>-1</sup> for SF-4800, which is consistent with our “overactivation” proposal. Sample SF-4600 has the

highest apparent surface area ever reported for activated carbons.<sup>16,88-96</sup> We are unaware of any reports of higher surface area (above  $4300 \text{ m}^2 \text{ g}^{-1}$ ) for activated carbons. We attribute this high apparent surface area to an optimal mix of KOH, the metal additives in the SF-hydrochar and an ideal activation temperature. The pore volume of the SF-4T carbons follows the same trend as surface area, being  $2.09 \text{ cm}^3 \text{ g}^{-1}$  for sample SF-4600, and decreasing to  $1.20 \text{ cm}^3 \text{ g}^{-1}$  for SF-4700 and  $1.09 \text{ cm}^3 \text{ g}^{-1}$  for SF-4800. It is noteworthy that despite the very high apparent surface area of sample SF-4600, it still exhibits an extremely high micropore surface area of  $3867 \text{ m}^2 \text{ g}^{-1}$ , which is 90% of the total surface area. This is the highest micropore surface area ever reported for an activated carbon.<sup>16,88-96</sup> Furthermore, the micropore volume that arises from micropores is also very high at 82% of total pore volume for sample SF-4600. The proportion of microporosity decreases at higher activation temperature in line with our over activation proposal.

### **3.3 Hydrogen storage**

As described above, all the carbons derived from fresh cigarette filters or used cigarette butts have high oxygen content, and some of the carbons also exhibit surface area that is amongst the highest ever reported for activated carbons. In addition, the highest surface area carbons also have very high microporosity with a significant proportion of porosity arising from small micropores of size  $< 1 \text{ nm}$ . Given that hydrogen storage in porous materials, and in particular porous carbons, is favoured by the presence of high surface area arising from micropores, we assessed the hydrogen uptake properties of the FF-4T and SF-4T samples. Our assessment conditions (i.e., storage capacity at  $-196 \text{ }^\circ\text{C}$  and pressure of  $0 - 40 \text{ bar}$ ) were chosen due to the fact that cryo-storage under such conditions is currently considered as viable for low pressure vehicular hydrogen storage.<sup>7,97-99</sup> For context, we note that, currently, apart from activated carbons,<sup>16-24,41,43,88-</sup>

<sup>92,100</sup> the best carbon-based hydrogen storage materials also include carbide-derived carbons (CDCs),<sup>28,47,57</sup> and zeolite templated carbons.<sup>21,25,52</sup>

The hydrogen uptake measured by a Hiden XEMIS analyser determined the excess hydrogen storage capacity from which we calculated the total storage capacity using established procedures (see Supporting Information, Appendix 1, for details on how excess and total hydrogen uptake were obtained). In our discussion, we refer to both the excess and total uptake as wt%, which are based on a dry material (carbon) basis. Figure 6 shows the excess and total hydrogen uptake isotherms at -196 °C, and the uptake at 1, 20, 30 and 40 bar is summarised in Table 2. We first note that the hydrogen uptake isotherms in all cases showed no hysteresis (Figure S5), which indicates that the hydrogen sorption process into the present activated carbons is reversible, which is similar to previous reports.<sup>16-24,41,43,88-92,100</sup> The hydrogen storage capacity at 1 bar ranges between 2 and up to 4 wt% (for sample SF-4600). An uptake of 4 wt% at 1 bar is impressive and at the top end of what has previously been reported for carbons.<sup>16-24,41,43,88-92,100</sup> A combination of the high apparent surface area, high microporosity in sample SF-4600 contributes to the high hydrogen uptake.

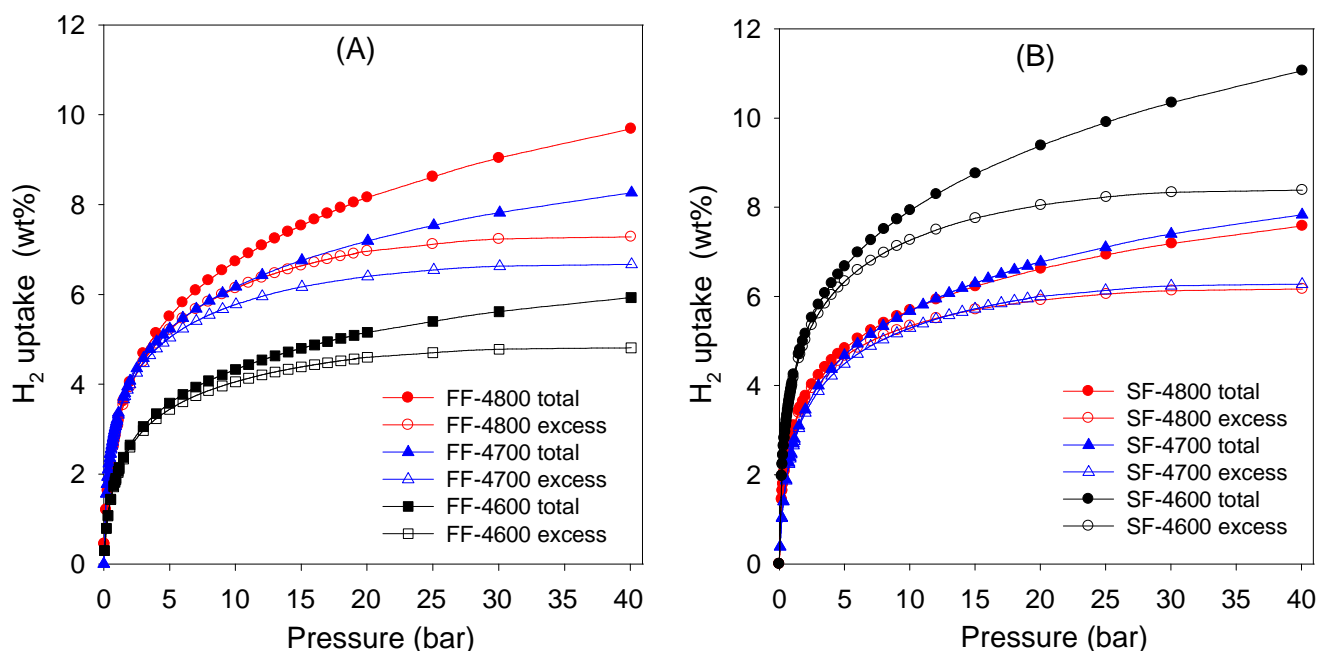


**Figure 6.** Excess and total hydrogen uptake at  $-196\text{ }^{\circ}\text{C}$  of activated carbons derived from (A) fresh cigarette filters and (B) smoked cigarette filters/butts. See experimental section for sample designation.

At 20 bar, the excess hydrogen uptake of FF-4T samples varies between 4.6 and 7.0 wt%, and increases with activation temperature in line with the rise in surface area. Excess hydrogen uptake (at 20 bar) of 6.4 wt% (FF-4700) and 7.0 wt% (FF-4800) is higher than most previously reported porous carbons.<sup>16-24,41,43,88-92,100</sup> The corresponding total uptake at 20 bar for FF-4T samples is 5.2 wt% (FF-4600), 7.2 wt% (FF-4700) and 8.2 wt% for FF-4800. For context, we note that amongst the best reported hydrogen uptake values under such conditions ( $-196\text{ }^{\circ}\text{C}$  and 20 bar) are; 7.03 wt%,<sup>46</sup> and 7.3 wt%,<sup>88</sup> for polypyrrole-derived activated and compactivated carbons, respectively, 7.08 wt% for a carbon that was both physically and chemically activated,<sup>41</sup> 8.1 wt%, for cellulose acetate derived activated carbons,<sup>22</sup> 7.1 wt%, for a sawdust-derived compactivated carbon,<sup>88</sup> and 7.3 wt% for a zeolite templated carbon.<sup>25</sup> Amongst the SF-4T carbons, the hydrogen uptake at 20 bar is similar to that of the FF-4T series except for sample SF-

4600 which has significantly higher excess and total uptake of 8.1 wt% and 9.4 wt%, respectively. Such uptake is unprecedented for porous carbons and far exceeds values reported to date.<sup>22,25,41,46,88</sup> The very high hydrogen uptake is attributable to the equally unprecedentedly high total and micropore surface area of sample SF-4600. As shown in Figure 6 and Table 2, the superior hydrogen uptake performance of SF-4600 is maintained at higher pressure, and the sample achieves total uptake of 10.4 wt% and 11.2 wt% at 30 and 40 bar, respectively.

It is well acknowledged that the weak interaction between adsorbed hydrogen and carbon surfaces can be improved via functionalization or doping with various heteroatoms.<sup>46,52,54,58,59,101</sup> Although the presence of O-functional groups (and thus an oxygen-rich surface) is not considered as doping, some studies suggest that they may afford an enhancing effect on atomic hydrogen adsorption.<sup>101-104</sup> In this regard, it was claimed that the hydrogen storage capacity of metal-doped carbons is enhanced due to the presence of oxygen functional groups,<sup>101</sup> and that oxygen-rich pillared graphene boron nitride have improved hydrogen storage capacity.<sup>104</sup> Regarding the adsorption of molecular hydrogen, which is more relevant to the present study, some previous studies have arrived at contradictory conclusions. Agarwal *et al.*<sup>105</sup> and Bleda-Martinez and co-workers,<sup>106</sup> claimed that high oxygen content causes an increase in hydrogen storage capacity while Huang *et al.*,<sup>107</sup> Schimmel *et al.*,<sup>108</sup> and Llorens and Pera-Titus<sup>109</sup> observed no positive effects. The conflicting claims may be explained by the fact that these previous studies<sup>105-109</sup> involved carbons for which both the oxygen content and textural properties varied to the extent that changes in one (oxygen content) caused variations in porosity (surface area, pore size and pore volume), for example via O-functional groups blocking micropores or limiting the space available for storage of hydrogen.<sup>110,111</sup> Such variation in both oxygen content and textural properties limits the ability to independently

determine the effect of either variable. The ambiguity may be eliminated by considering how large,<sup>22</sup> rather than small,<sup>112</sup> variations in oxygen content influence hydrogen uptake in carbons with similar pore size or porosity. We have recently shown that whilst porosity is the main determinant of hydrogen storage capacity, it is also the case that at any given level of porosity, oxygen-rich carbons exhibit enhanced gravimetric hydrogen storage uptake compared to relatively oxygen-poor samples of similar porosity.<sup>22</sup> In the present study, for completeness, we compared the hydrogen uptake of sample SF-4800 to that of a cellulose-derived activated carbon (designated as C-4700),<sup>20</sup> which has similar porosity (Figure S5 and Table S2) but much lower oxygen content (Supporting Figure S1). Such a comparison eliminates any ambiguities and can clarify on the effect of oxygen content. The total surface area and pore volume of the two samples is identical and their pore size is very similar (Table S2 and Supporting Figure S5). The main difference is that sample SF-4800 has a much higher oxygen content of 16.4 wt% compared to 7.1 wt% for C-4700. Despite the similarity in porosity, the O-rich sample (SF-4800) has much higher hydrogen uptake (Figure S6); at 1 bar the uptake of SF-4800 (3.0 wt%) is higher than for C-4700 (2.5 wt%). At 20 bar the excess uptake of SF-4800 is 5.9 wt%, which is 20% higher than 4.9 wt% for C-4700. We tentatively ascribe the higher hydrogen storage capacity of the SF-4800 sample to a higher oxygen content, which is consistent with previous finding on the interaction between H and O-rich carbon surfaces.<sup>104,113,114</sup>

The gravimetric hydrogen uptake of the best performing carbons (SF-4800 and SF-4600), at pressures of up to 30 bar, is better than that of MOF materials that are currently the best hydrogen stores.<sup>34,36,37</sup> This is depicted in Figure 7, and the relevant data is summarised in Table S3. This is despite the fact that the MOFs possess much higher surface area (Table S3). At 20 bar, the excess hydrogen storage capacity of sample SF-4600 (8.1 wt%) is higher than that of high surface area MOFs such as NOTT-112 (6.9

wt%),<sup>34</sup> NU-100 (6.8 wt%)<sup>36</sup> and MOF-210 (6.4 wt%),<sup>37</sup> which are the current record holders for gravimetric hydrogen storage in porous materials under cryogenic conditions. The total hydrogen uptake of SF-4600 (9.4 wt%), at 20 bar, is also higher than that of NOTT-112 (7.8 wt%),<sup>34</sup> NU-100 (8.5 wt%)<sup>36</sup> and MOF-210 (8.4 wt%).<sup>37</sup> We postulate that the superior hydrogen storage capacity of sample SF-4600, despite having lower apparent surface area, may be explained in part by the high oxygen content and that an oxygen-rich surface is attractive for adsorption of molecular hydrogen, and thus compensates for the lower surface area compared to the MOFs. At 30 bar, the hydrogen uptake capacity of SF-4600 still outperforms that of the MOFs (Figure 7 and Table S3). In addition to their impressive storage capacity, the present carbons also offer all the advantages of carbons such as easy processing, high mechanical and chemical stability along with ease of preparation and low cost, in addition to the valorisation and environmental protection aspects associated with using cigarette butts as starting materials.

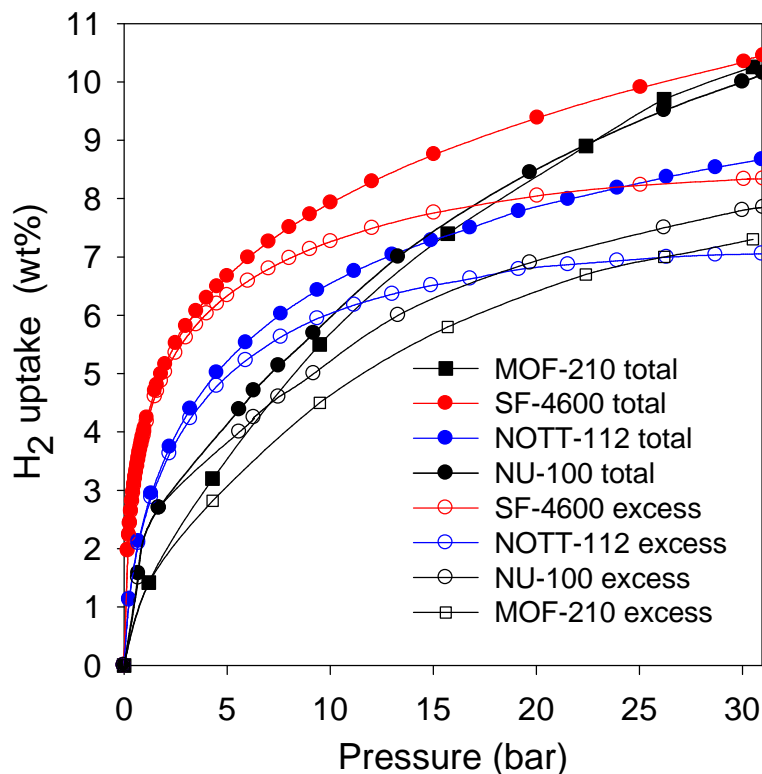


**Figure 7.** Excess and total gravimetric hydrogen uptake of activated carbon (SF-4600) derived from smoked cigarette butts compared to the best benchmark high surface area metal organic frameworks (MOFs), namely, NOTT-112,<sup>34</sup> NU-100,<sup>36</sup> and MOF-210.<sup>37</sup>

#### 4. Conclusions

Hydrothermal carbonisation of cigarette filters and discarded (i.e., smoked) cigarette butts yields hydrochar, which when activated generates oxygen-rich (with oxygen functional groups such as COOH, C-OH and O-C=O) porous carbons that have extremely high apparent surface area (up to  $4300 \text{ m}^2 \text{ g}^{-1}$ ) with most of the surface area (up to  $3867 \text{ m}^2 \text{ g}^{-1}$ ), i.e. 90%, arising from micropores. The carbons derived from smoked cigarette butts show anomalous behaviour with respect to the effect of activation temperature on their porosity, i.e., highest surface area and pore volume at  $600 \text{ }^\circ\text{C}$ , which then decreases for samples activated at higher temperature. The anomalous trend is explained by the presence of significant amounts of

metal additives in the cigarette butt-derived hydrochar used as starting material; the metal additives (K, Ca, Na, Mg, etc) themselves act as activating agent in addition to the added KOH. Due to the combined effects of high surface area, high microporosity and an oxygen-rich nature, the carbons exhibit unprecedentedly high hydrogen storage capacity of 8.1 wt% excess uptake, and 9.4 wt% total uptake at -196 °C and 20 bar, rising to total uptake of 10.4 wt% and 11.2 wt% at 30 and 40 bar, respectively. Our findings offer new insights on the valorisation of a major waste disposal and environmental pollution hazard (discarded cigarette butts) to attractive energy materials with, in the present case, the highest hydrogen uptake capacity reported to date for any carbons or porous materials in general. The findings therefore have direct relevance to an environmental pollution issue and offer a new research direction in the search for carbon-based sustainable energy storage materials, and not least raise the interesting question of whether valorisation can solve the intractable cigarette butt problem.

## **Supporting Information**

Supporting information accompanying this paper, including details of calculation of total hydrogen uptake, and three tables and six figures is available.

## **Acknowledgements**

We are grateful to Dr Isabel Vicente and Dr Gual Gozalbo Aitor for assistance with TPD measurements. This work was supported by the Engineering and Physical Sciences Research Council [grant number EP/M000567/1] for the Nottingham Gas Adsorption Analysis Suite. RM thanks the Royal Society for a Research Grant (AQ150029), and for a Royal Society Wolfson Research Merit Award.

## References

1. J. A. Turner, *Science*, 1999, **285**, 687.
2. C-J. Winter, *Int. J. Hydrogen Energy*, 2009, **34**, S1 - S52.
3. J. Andrews and B. Shabani, *Int. J. Hydrogen Energy*, 2012, **74**, 1184.
4. P. Moriarty and D. Honnery, *Int. J. Hydrogen Energy*, 2009, **34**, 31.
5. L. Schlapbach and A. Züttel, *Nature*, 2001, **414**, 353.
6. G. W. Crabtree, M. S. Dresselhaus and M. V. Buchanan, *Phys. Today*, 2004, **57**, 39.
7. U. Eberle, B. Muller and R. von Helmut, *Energy Environ. Sci.*, 2012, **5**, 8780.
8. R. P. O'Hayre, S.-W. Cha, W. Colella and F. B. Prinz, *Fuel cell fundamentals*, John Wiley & Sons New York, 2006.
9. A. Cho, *Science*, 2004, **305**, 964.
10. R. von Helmut and U. Eberle, *J. Power Sources*, 2007, **165**, 833.
11. <http://energy.gov/eere/fuelcells/hydrogen-storage>, (accessed June 2017).
12. D. Pukazhselvan, V. Kumar, S. K. Singh, *Nano Energy*, 2012, **1**, 566.
13. P. Jena, *J. Phy. Chem. Lett.*, 2011, **2**, 206.
14. A. W. C. van den Berg and C. O. Arean, *Chem. Commun.*, 2008, 668.
15. I. P. Jain, P. Jain, A. Jain, *J. Alloys Compds*, 2010, **503**, 303.
16. M. Sevilla and R. Mokaya, *Energy Environ. Sci.*, 2014, **7**, 1250.
17. J. Burrell, M. Kraus, M. Beckner, R. Cepel, C. Wexler and P. Pfeifer, *Nanotechnology*, 2009, **20**, 204026.
18. J. Juan-Juan, J. P. Marco-Lozar, F. Suarez-Garcia, D. Cazorla-Amoros and A. Linares-Solano, *Carbon*, 2010, **48**, 2906.
19. C. Wang and S. Kaskel, *J. Mater. Chem.*, 2012, **22**, 23710.
20. M. Sevilla, A. B. Fuertes and R. Mokaya, *Energy Environ. Sci.*, 2011, **3**, 1400.
21. Z. Yang, Y. Xia and R. Mokaya, *J. Am. Chem. Soc.*, 2007, **129**, 1673.
22. T. S. Blankenship, N. Balahmar and R. Mokaya, *Nat. Commun.*, 2017, NCOMMS-17-11777.
23. G. Sethia and A. Sayari, *Carbon*, 2016, **9**, 289.
24. M. Jordá-Beneyto, F. Suárez-García, D. Lozano-Castelló, D. Cazorla-Amorós, A. Linares-Solano, *Carbon*, 2007, **45**, 293.
25. E. Masika and R. Mokaya, *Energy Environ. Sci.*, 2014, **7**, 427.
26. N. Balahmar, A. M. Lowbridge and R. Mokaya, *J. Mater. Chem. A*, 2016, **4**, 14254.

27. M. de la Casa-Lillo, F. Lamari-Darkrim, D. Cazorla-Amoros and A. Linares-Solano, *J. Phys. Chem. B*, 2002, **106**, 10930.
28. M. Sevilla, R. Foulston and R. Mokaya, *Energy Environ. Sci.*, 2010, **3**, 223.
29. N. Alam and R. Mokaya, *Energy Environ. Sci.*, 2010, **3**, 1773.
30. E. Poirier, R. Chahine and T. K. Bose, *Int. J. Hydrogen Energy*, 2001, **26**, 831.
31. S. S. Kaye, A. Dailly, O. M. Yaghi and J. R. Long, *J. Am. Chem. Soc.*, 2007, **129**, 14176.
32. H. W. Langmi, J. W. Ren, B. North, M. Mathe, D. Bessarabov, *Electrochimica Acta*, 2014, 128, 368.
33. L. J. Murray, M. Dincă and J. R. Long, *Chem. Soc. Rev.*, 2009, **38**, 1294.
34. Y. Yan, X. Lin, S. Yang, A. J. Blake, A. Dailly, N. R. Champness, P. Hubberstey and M. Schroder, *Chem. Commun.*, 2009, 1025.
35. S. Y. Ding and W. Wang, *Chem. Soc. Rev.*, 2013, **42**, 548.
36. O. K. Farha, A. O. Yazaydin, I. Eryazici, C. D. Malliakas, B. G. Hauser, M. G. Kanatzidis, S. T. Nguyen, R. Q. Snurr and J. T. Hupp, *Nat. Chem.*, 2010, **2**, 944.
37. H. Furukawa, N. Ko, Y. B. Go, N. Aratani, S. B. Choi, E. Choi, A. O. Yazaydin, R. Q. Snurr, M. O'Keeffe, J. Kim and O. M. Yaghi, *Science*, 2010, **329**, 424.
38. S. S. Han, H. Furukawa, O. M. Yaghi and W. A. Goddard, *J. Am. Chem. Soc.*, 2008, **130**, 11580.
39. H. Furukawa and O. M. Yaghi, *J. Am. Chem. Soc.*, 2009, **131**, 8875.
40. E. Klontzas, E. Tylianakis and G. E. Froudakis, *Nano Lett.*, 2010, **10**, 452.
41. H. Wang, Q. Gao and J. Hu, *J. Am. Chem. Soc.*, 2009, **131**, 7016.
42. A. Almasoudi and R. Mokaya, *J. Mater. Chem.*, 2012, **22**, 146.
43. B. Panella, M. Hirscher and S. Roth, *Carbon*, 2005, **43**, 2209.
44. Y. Xia and R. Mokaya, *J. Phys. Chem. C*, 2007, **111**, 10035.
45. E. Masika and R. Mokaya, *J. Phys. Chem. C*, 2012, **116**, 25734.
46. M. Sevilla, R. Mokaya and A. B. Fuertes, *Energy Environ. Sci.*, 2011, **4**, 2930.
47. Y. Gogotsi, R. K. Dash, G. Yushin, T. Yildirim, G. Laudisio and J. E. Fischer, *J. Am. Chem. Soc.*, 2005, **127**, 16006.
48. N. Alam and R. Mokaya, *Micropor. Mesopor. Mater.*, 2011, **142**, 716.
49. O. K. Farha, I. Eryazici, N. C. Jeong, B. G. Hauser, C. E. Wilmer, A. A. Sarjeant, R. Q. Snurr, S. T. Nguyen, A. Ö. Yazaydin and J. T. Hupp, *J. Am. Chem. Soc.*, 2012, **134**, 15016.
50. C. Robertson and R. Mokaya, *Micropor. Mesopor. Mater.* 2013, **179**, 151.

51. H. Tanaka, H. Kanoh, M. Yudasaka, S. Iijima and K. Kaneko, *J. Am. Chem. Soc.*, 2005, **127**, 7511.
52. Y. Xia, G. S. Walker, D. M. Grant and R. Mokaya, *J. Am. Chem. Soc.*, 2009, **131**, 16493.
53. A. Almasoudi and R. Mokaya, *J. Mater. Chem. A*, 2014, **2**, 10960.
54. M. Sevilla, A. B. Fuertes and R. Mokaya, *Int. J. Hydrogen Energy*, 2011, **36**, 15658.
55. N. Alam and R. Mokaya, *Micropor. Mesopor. Mater.*, 2011, **144**, 140
56. Z. Yang, Y. Xia, X. Sun and R. Mokaya, *J. Phy. Chem. B*, 2006, **110**, 18424.
57. G. Yushin, R. Dash, J. Jagiello, J. E. Fischer and Y. Gogotsi, *Adv. Funct. Mater.*, 2006, **16**, 2288.
58. Y. Xia, R. Mokaya, D. M. Grant and G. S. Walker, *Carbon*, 2011, **49**, 844.
59. E. Masika, R. A. Bourne, T. W. Chamberlain and R. Mokaya, *ACS Appl. Mater. Interfaces*, 2013, **5**, 5639.
60. P. Wexler, *Encyclopedia of Toxicology, Four-Volume Set*, ACADEMIC Press INC, 2005.
61. E. Lassner, W.-D. Schubert, E. Lüderitz and H. U. Wolf, in *Ullmann's Encyclopedia of Industrial Chemistry*, Wiley-VCH Verlag GmbH & Co. KGaA, 2000, DOI: 10.1002/14356007.a27\_229.
62. H. Moriwaki, S. Kitajima, K. Katahira, *Waste Manage.*, 2009, **29**, 1192.
63. E. A. Smith and T. E. Novotny, *Tob Control*, 2011, **20**, i2 – i9.
64. B. Harris, *Tob Control*, 2011, **20**, i10 – i16.
65. T. E. Novotny, S. N. Hardin, L. R. Hovda, D. J. Novotny, M. K. McLean and S. Khan, *Tob Control*, 2011, **20**, i17 – i20.
66. E. Slaughter, R. M. Gersberg, K. Watanabe, J. Rudolph, C. Stransky and T. E. Novotny, *Tob Control*, 2011, **20**, i25 – i29.
67. J. Puls, S. A. Wilson and D. Hölter, *J. Polym. Environ.*, 2011, **19**, 152.
68. <http://www.tobaccoatlas.org/topic/cigarette-use-globally/> (Accessed June 2017).
69. T. E. Novotny, K. Lum, E. Smith, V. Wang and R. Barnes, *Int. J. Environ. Res. Public Health*, 2009, **6**, 1691.
70. J. W. Moerman and G. E. Potts, *Tob Control*, 2011, **20**, i30-i35.
71. F. Y. Iskander, T. L. Bauer and D. E. Klein, *Analyst*, 1986, **3**, 107.
72. P. Bell and C. L. Mulchi, *Tob Sci.*, 1990, **34**, 32.
73. S. Polarz, B. Smarsly and J. H. Schattka, *Chem. Mater.*, 2002, **14**, 2940.

74. A. Chen, Y. Li, Y. Yu, Y. Li, L. Zhang, H. Lv and L. Liu, *RSC Adv.*, 2015, **5**, 107299.
75. M. Lee, G. P. Kim, H. Don Song, S. Park and J. Yi, *Nanotechnology*, 2014, **25**, 345601.
76. M. C. Tellez-Juarez, V. Fierro, W. Zhao, N. Fernandez-Huerta, M. T. Izquierdo, E. Reguera and A. Celzard, *Int. J. Hydrogen Energy*, 2014, **39**, 4996.
77. J. L. Figueiredo, M. F. R. Pereira, M. M. A. Freitas, J. J. M. Orfao, *Carbon*, 1999, **37**, 1379.
78. J. L. Figueiredo, M. F. R. Pereira, *Catal. Today*, 2010, **150**, 2.
79. M. Sevilla and A.B. Fuertes, *Carbon*, 2009, **47**, 2281.
80. J. Romanos, M. Beckner, T. Rash, L. Firlej, B. Kuchta, P. Yu, G. Suppes, C. Wexler and P. Pfeifer, *Nanotechnology*, 2012, **23**, 015401.
81. Y. Zhao, W. Ran, J. He, Y. Song, C. Zhang, D. B. Xiong, F. Gao, J. Wu and Y. Xia, *ACS Appl. Mater. Interfaces*, 2015, **7**, 1132.
82. H. Wang and Y. H. Hu, *Ind. Eng. Chem. Res.*, 2011, **50**, 6132.
83. K. S. W. Sing, D. H. Everett, R. A. W. Haul, L. Moscou, R. A. Pierotti, J. Rouquerol and T. Siemieniewska, *Pure Appl. Chem.*, 1985, **57**, 603.
84. H. M. Coromina, D. A. Walsh and R. Mokaya, *J. Mater. Chem. A*, 2016, **4**, 280.
85. H. M. Coromina, B. Adeniran, R. Mokaya and D. A. Walsh and, *J. Mater. Chem. A*, 2016, **4**, 14586.
86. N. Balahmar, A. Al-Jumialy and R. Mokaya, *J. Mater. Chem. A*, 2017, **5**, 12330.
87. B. Adeniran and R. Mokaya, *Chem. Mater.* 2016, **28**, 994.
88. B. Adeniran and R. Mokaya, *Nano Energy*, 2015, **16**, 173.
89. W. Sangchoom and R. Mokaya, *ACS Sust. Chem. Eng.*, 2015, **3**, 1658.
90. B. Adeniran and R. Mokaya, *J. Mater. Chem. A*, 2015, **3**, 5148.
91. B. Adeniran, E. Masika and R. Mokaya, *J. Mater. Chem. A*, 2014, **2**, 14696.
92. A. Almasoudi and R. Mokaya, *Micropor. Mesopor. Mater.*, 2014, **195**, 258.
93. N. Balahmar, A. C. Mitchell, and R. Mokaya, *Adv. Energy Mater.*, 2015, **5**, 1500867.
94. M. Sevilla, W. Sangchoom, N. Balahmar, A. B. Fuertes and R. Mokaya, *ACS Sust. Chem. Eng.*, 2016, **4**, 4710.
95. J. He, J. W. F. To, P. C. Psarras, H. Yan, T. Atkinson, R. T. Holmes, D. Nordlund, Z. Bao and J. Wilcox, *Adv. Energy Mater.*, 2016, **6**, 1502491.
96. A. S. Jalilov, Y. Li, J. Tian and J. M. Tour, *Adv. Energy Mater.*, 2017, **7**, 1600693.

97. D. A. Gomez-Gualdron, Y. J. Colón, X. Zhang, T. C. Wang, Y. Chen, J. T. Hupp, T. Yildirim, O. K. Farha, J. Zhang and R. Q. Snurr, *Energy Environ. Sci.*, 2016, **9**, 3279.
98. [http://energy.gov/sites/prod/files/2015/05/f22/fcto\\_myRDD\\_storage.pdf](http://energy.gov/sites/prod/files/2015/05/f22/fcto_myRDD_storage.pdf), accessed Jan. 2017.
99. U. Eberle and R. von Helmolt, *Energy Environ. Sci.*, 2010, **3**, 689.
100. M. Jorda-Beneyto, D. Lozano-Castello, F. Suarez-Garcia, D. Cazorla-Amoros and A. Linares-Solano, *Micropor. Mesopor. Mater.*, 2008, **112**, 235.
101. Z. Wang, F. H. Yang and R. T. Yang, *J. Phys. Chem. C*, 2010, **114**, 1601.
102. L. Wang, F. H. Yang, R. T. Yang and M. A. Miller, *Ind. Eng. Chem. Res.*, 2009, **48**, 2920.
103. Q. Li, and A. D. Lueking, *J. Phys. Chem. C*, 2011, **115**, 4273.
104. F. Shayeganfar and R. Shahsavari, *Langmuir*, 2016, **32**, 13313.
105. R. K. Agarwal, J. S. Noh, J. A. Schwarz and R. Davini, *Carbon*, 1987, **25**, 219.
106. M. J. Bleda-Martinez, J. M. Perez, A. Linares-Solano, E. Morallon and D. Cazorla-Amoros, *Carbon*, 2008, **46**, 1053.
107. C. C. Huang, H. M. Chen, C. H. Chen and J. C. Huang, *Sep. Purif. Technol.*, 2010, **70**, 291.
108. H. G. Schimmel, G. Nijkamp, G. J. Kearley, A. Rivera, K. P. De Jong and F. M. Mulder, *Mater. Sci. Eng. B*, 2004, **108**, 124.
109. J. Llorens and M. Pera-Titus, *Colloids Surf. A*, 2009, **350**, 63.
110. M. Georgakis, G. Stavropoulos and G. P. Sakellariopoulos, *Int. J. Hydrogen Energy*, 2007, **32**, 1999.
111. H. Takagi, H. Hatori, Y. Yamada, S. Matsuo and M. Shiraishi, *J. Alloys Compd*, 2004, **385**, 257.
112. M. C. Tellez-Juarez, V. Fierro, W. Zhao, N. Fernandez-Huerta, M. T. Izquierdo, E. Reguera and A. Celzard, *Int. J. Hydrogen Energy*, 2014, **39**, 4996.
113. Z. Wang, F. H. Yang and R. T. Yang, *J. Phys. Chem. C*, 2010, **114**, 1601.
114. L. Wang, F. H. Yang, R. T. Yang and M. A. Miller, *Ind. Eng. Chem. Res.*, 2009, **48**, 2920.

## Graphical Abstract

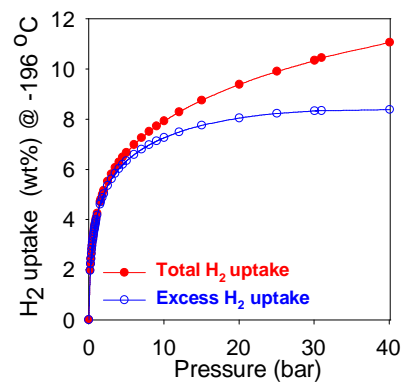
Cigarette butt derived carbons are highly porous ( $4310 \text{ m}^2 \text{ g}^{-1}$  and  $2.09 \text{ cm}^3 \text{ g}^{-1}$ ) with record levels of hydrogen storage.



Hydrothermal  
Carbonisation  
Activation



Activated  
Carbon (AC)



## Broader Context

This manuscript not only addresses an intractable environmental pollution problem – cigarette butts – and also offers new insights on a valorisation route to the best performing hydrogen storage materials to date as part of the drive towards the anticipated Hydrogen Economy wherein efficient storage and transportation of hydrogen are key to exploitation of hydrogen as an energy source. Discarded cigarette filters, in the form of cigarette butts, are a major waste disposal and environmental pollution hazard due to the fact that they are mainly composed of cellulose acetate which is non-biodegradable. The problem is huge; 5.8 trillion cigarettes are smoked worldwide per annum generating > 800 000 metric tons of cigarette butts. Apart from causing unsightly litter, cigarette butts contain contaminants such as toxic heavy metals, which can leach into waterways, potentially causing harm to both humans and wildlife. In an effort to turn such undesirable and dangerous waste into value products, this study explores the valorisation of discarded smoked cigarette filters/butts. We show that porous carbons derived from cigarette butts, via sequential benign hydrothermal carbonisation and activation, are super porous with ultra-high surface area ( $4300 \text{ m}^2 \text{ g}^{-1}$ ) and pore volume ( $2.09 \text{ cm}^3 \text{ g}^{-1}$ ), and exhibit unprecedentedly high hydrogen storage capacity. This work, therefore, not only raises the interesting question of whether valorisation can solve the intractable *cigarette butt problem* but also offers hydrogen storage materials that attain new levels for porous materials in general.